Bioinspiration & Biomimetics

PAPER

RECEIVED
25 January 2016

REVISED
6 May 2016

ACCEPTED FOR PUBLICATION
7 June 2016

PUBLISHED
5 July 2016

Mechanisms of anguilliform locomotion in fishes studied using simple three-dimensional physical models

Jeanette L Lim[1] **and George V Lauder**

Department of Organismic & Evolutionary Biology, Harvard University, 26 Oxford St, Cambridge, MA, 02138, USA
[1] Current address: The Biomimicry Institute, PO Box 9216, Missoula, MT, 59807, USA.

E-mail: jeanettelim@post.harvard.edu

Keywords: anguilliform, undulatory swimming, hagfish, physical model, particle image velocimetry, flexibility

Abstract

Physical models enable researchers to systematically examine complex and dynamic mechanisms of underwater locomotion in ways that would be challenging with freely swimming animals. Previous research on undulatory locomotion, for example, has used rectangular flexible panels that are effectively two-dimensional as proxies for the propulsive surfaces of swimming fishes, but these bear little resemblance to the bodies of elongate eel-like swimming animals. In this paper we use a polyurethane rod (round cross-section) and bar (square cross-section) to represent the body of a swimming Pacific hagfish (*Eptatretus stoutii*). We actuated the rod and bar in both heave and pitch using a mechanical controller to generate a propulsive wave at frequencies between 0.5 and 2.5 Hz. We present data on (1) how kinematic swimming patterns change with driving frequency in these elongate fish-like models, (2) the thrust-generating capability of these simple models, (3) how forces and work done during propulsion compare between cross-sectional shapes, (4) the wake flow patterns in these swimming models using particle image velocimetry. We also contrast kinematic and hydrodynamic patterns produced by bar and rod models to comparable new experimental data on kinematics and wake flow patterns from freely swimming hagfish. Increasing the driving frequency of bar and rod models reduced trailing edge amplitude and wavelength, and above 2 Hz a nodal point appeared in the kinematic wave. Above 1 Hz, both the rod and bar generated net thrust, with the work per cycle reaching a minimum at 1.5 Hz, and the bar always requiring more work per cycle than the rod. Wake flow patterns generated by the swimming rod and bar included clearly visible lateral jets, but not the caudolaterally directed flows seen in the wakes from freely swimming hagfish.

1. Introduction

When experimental research with live swimming animals presents logistical and behavioral constraints, physical models can be used to more systematically explore the often complex and dynamic mechanisms of underwater locomotion (e.g., McHenry *et al* 1995, Root *et al* 1999, Lauder *et al* 2011, Leftwich *et al* 2012). Engineers and biologists alike have found immense utility in using physical models that simplify biological complexity. Plastic or rubber flexible panels, simple rigid plates, or models of animal shape (review of biomechanical modeling in Koehl 2003, also see Emerson *et al* 1990, Johansson and Norberg 2003, Koehl *et al* 2011, Richards and Clemente 2012, Blevins and Lauder 2013, Dewey *et al* 2013) all have provided an avenue for analyzing a simpler mechanical system that contains key elements of a multidimensional biological configuration. The adjustable physical properties and relative ease of control and operation of simple models have enabled systematic study of how aquatic locomotion is affected by an array of variables including body morphology, kinematics, stiffness, and fluid forces.

Flexible panels in particular have been widely used to serve as proxies for the propulsive parts of a swimming organism, be it a fin or an undulating body, but the two-dimensional, often rectangular shape of these models typically bears little resemblance to a whole, swimming animal. At the other end of the spectrum are physical models that closely replicate a live organism's morphology and behavior. Examples include a

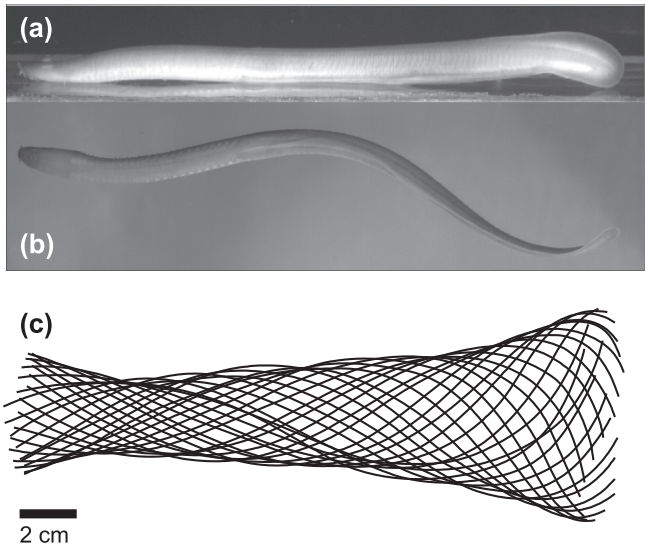

Figure 1. (a) Lateral and (b) ventral views of a Pacific hagfish (*Eptatretus stoutii*) swimming steadily in the experimental flow tank. (c) Ventral body midline tracings from Pacific hagfish (*Eptatretus stoutii*) swimming at 0.52 body lengths/second (BL s^{-1}) with a tail beat frequency of 0.97 Hz. A series of traced midlines from sequential instances in time, each separated by $\Delta t = 0.04$ s, are overlaid on top of one another to indicate the lateral amplitude envelope for a typical whole tail beat cycle. Modified from Lim and Winegard (2015).

large robotic bluegill sunfish fin complete with tendon-like strings that control fin movement (Tangorra *et al* 2010), a robotic knifefish with undulating anal fin (Curet *et al* 2011), a lamprey-inspired swimming robot (Leftwich *et al* 2012), and a mackerel-shaped robot capable of adopting different modes of body and caudal fin swimming (Wen *et al* 2012). Unsurprisingly, a cost of this increased realism is that these models are more complicated to build, operate, and iterate when design changes are needed.

Elongate, anguilliform (eel-like) swimmers present a unique opportunity to balance this trade-off between simplicity and biological realism. In this paper, we explore anguilliform aquatic locomotion in fishes using physical models that are simple in shape and to control, but that are three-dimensional and represent a reasonable approximation of an elongate eel-like swimming fish. Anguilliform locomotion in fishes is common to many elongate species and is often defined as occurring when more than one wavelength of body bending is present at any given time (e.g., Webb 1975, Lindsey 1978). This mode of swimming has been studied in a number of species, including hagfish (Long *et al* 2002, Lim and Winegard 2015), eels (Gillis 1998, Tytell 2004), lamprey (Tytell *et al* 2010, Dabiri *et al* 2014, Gemmell *et al* 2015, Williams and McMillen 2015), and swimming snakes (Jayne 1985, Munk 2008). Hagfishes (Myxinidae) are anguilliform swimmers that are particularly well-approximated by simple physical models. Their bodies, which are mostly cylindrical with some lateral compression toward the caudal end (figure 1; Hart 1973), lack discrete fins and a fully developed vertebral column, retaining a flexible cartilaginous notochord into adulthood instead (Long *et al* 2002, Ota *et al* 2011). As a result, there is relatively little variation in body flexibility along the length of hagfish, and rod-like approximations are a reasonable first approach to understand patterns of body oscillation which have recently been studied experimentally in live hagfish (Lim and Winegard 2015).

We used a polyurethane rod (with a round cross-section) and bar (with a square cross-section) to represent the body of a generalized elongate anguilliform swimmer and for specific comparison to new data presented here on swimming hagfish. We actuated these two models in heave (lateral translation; termed 'sway' in a ship) and pitch (rotation about a vertical axis; termed 'yaw' in a ship) at their anterior end (leading edge) only, and did not include the effect of active muscular contraction that is present along the length of a live swimming fish's body. Previous work on the propulsion of passive models (e.g., Alben 2008, Lauder *et al* 2011, Moored *et al* 2012, Dewey *et al* 2013, Shelton *et al* 2014, Lucas *et al* 2015, Quinn *et al* 2015) has used rectangular flexible plastic panels with an aspect ratio (length to height) ranging from 1 to 4 to represent swimming flexible bodies, and these panels have been effectively two-dimensional with thickness being only a small fraction (<1%) of their length. Here we extend this work to a simple rod-like system with a much higher aspect ratio and clear three-dimensionality. Any undulatory 'body' waves present on the rod-like models are generated at the leading edge and then passively propagated down the model as they interact with surrounding fluid.

Our overall goal is to explore several features of anguilliform propulsion not possible with *in vivo* analyses. Specifically, we present data on (1) how kinematic swimming patterns change with driving frequency in

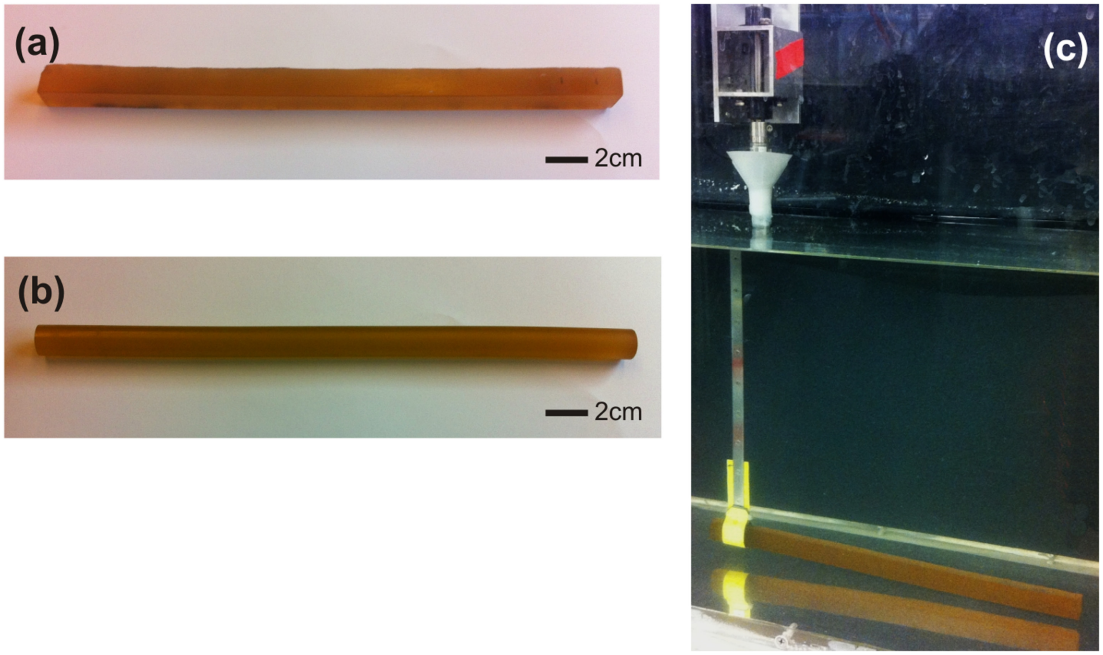

Figure 2. Simple physical models approximating elongate anguilliform swimmers. (a) Polyurethane bar with a square cross-section (1.6 cm on each side). (b) Polyurethane rod with a circular cross-section (1.6 cm diameter). (c) The polyurethane bar in the variable-speed flow tank, attached to a robotic control device and six-axis force/torque sensor via a metal shaft and holster encircling the model. There is a reflection of the bar model from the bottom of the flow tank in panel (c), and when actuated in flow the posterior end lifts off the bottom.

these fish-like models, expecting their bending behavior to reflect mechanical wave theory; (2) the thrust-generating capability of these simple models, which we expected could generate thrust through passively propagated body waves; (3) how forces and work done during propulsion compare between cross-sectional shapes, predicting that the bar would generate increased thrust relative to the rod; and (4) the wake flow patterns in these swimming models using particle image velocimetry (PIV). Here, we expected the physical models' wakes to consist of alternating fluid jets. We contrast the kinematic and hydrodynamic patterns produced by the bar and rod models to comparable new experimental data on kinematics and wake flow patterns from freely swimming hagfish.

2. Materials and methods

2.1. Experimental animals

Pacific hagfish (*Eptatretus stoutii*, Lockington) were collected in baited traps from Barkley Sound, British Columbia, with assistance from the Bamfield Marine Sciences Centre. The hagfish were transported to an aquarium facility at Harvard University and maintained in a recirculating artificial seawater tank (8 °C–9 °C, 35‰ salinity) on a 12 h light:12 h dark cycle while fed frozen squid monthly. Swimming behaviors were recorded from four individuals ranging from 23.0–30.3 cm in body length (BL) (mean BL ± standard deviation, 28.0 ± 3.4 cm), and body depth ranged from 1 cm near the head to approximately 1.5 cm at the tail (figure 1). All procedures and experiments were conducted in accordance with Harvard University IACUC animal care guidelines (protocol # 20-03).

2.2. Simple anguilliform models and robotic controller

Polyurethane bars (square cross-section) and rods (circular cross-section) (40A durometer, McMaster-Carr, Robbinsville, NJ) (see figures 2(a) and (b)) served as simple three-dimensional physical models of elongate anguilliform swimmers. Bars and rods were chosen to correspond in dimensions to the larger live hagfish individuals studied, both in length and body depth. The bars measured 1.6 cm on each side, and the diameter of the rods was 1.6 cm; the length of both the rod and bar was 30.5 cm. As many elongate swimmers have bodies that are cylindrical in anterior regions and laterally flattened in posterior regions (e.g., hagfish (Hart 1973), freshwater eels (Scott and Scott 1988), aquatic snakes (Brischoux and Shine 2011)), these models represent opposite simplified extremes in elongate body shape. Due to their identical heights, the rod and bar models have the same lateral projected area but they differ in total mass and flexural stiffness (rod: 5.9×10^{-3} Nm^2; bar: 9.4×10^{-3} Nm^2). These values are somewhat higher than flexural stiffness measurements previously reported for similarly shaped elongate anguilliform swimmers, but still within a range that includes other body and caudal fin-mode swimmers (table 1).

Table 1. Body flexural stiffness measurements for several elongate undulatory swimming models (this paper) and fishes.

Model/Species	Flexural stiffness, EI (Nm^2)	Source
Polyurethane (round) rod	5.9×10^{-3}	Present study
Polyurethane (square) bar	9.4×10^{-3}	Present study
Hagfish (*Myxine glutinosa*)	3.0×10^{-4}	Long *et al* (2002)
American eel (*Anguilla rostrata*)		
Eel electrically stimulated (active)	$3.0–5.6 \times 10^{-4}$	Long (1998)
Eel unstimulated (passive)	$1.5–2.0 \times 10^{-4}$	Long (1998)
Longnose gar (*Lepisosteus osseus*)	6.5×10^{-2}	Long *et al* (1996)

A custom-built mechanical device was used to actuate each physical model in a variable-speed flow tank filled with freshwater (84 × 28 × 28 cm working section). A detailed description of this mechanical flapping apparatus is provided in our previous work (e.g., Alben 2008, Lauder *et al* 2011, Shelton *et al* 2014, Feilich and Lauder 2015, Lucas *et al* 2015, Quinn *et al* 2015, Witt *et al* 2015), and only a brief description of the relevant components is given here. Heave and pitch motors controlled with a custom LabView (v. 8, National Instruments, Austin, TX) interface are mounted above the recirculating flow tank, where they attach to the physical model submerged in the water via a metal shaft (figure 2(c)). The model was attached to the shaft via a metal holster wrapped around the model's diameter approximately 1 cm behind the leading edge, with the model's midline positioned approximately 1.5 cm above the bottom of the flow tank. This placement was chosen to approximate the bottom-swimming commonly observed in hagfish (Lim and Winegard 2015) and eels (Tytell and Lauder 2004). The boundary layer for this flow tank was found to be 0.2–0.7 cm thick at flow speeds comparable to the highest speeds used in the present study (Tytell and Lauder 2004, Carlson and Lauder 2011). Because boundary layers become thicker as flow speeds decrease (Schlichting 1979), it is possible that boundary layer flows influenced the model's swimming; however, because the main focus of this study is on comparisons between physical models and between the models and swimming hagfish, the potential effect of swimming near the bottom is not considered here as rod and bar models and hagfish experienced the same flow conditions. Also, near-bottom or wall effects on undulatory swimming in this same experimental flow tank have been explored previously by Quinn *et al* (2014) and Blevins and Lauder (2013).

2.3. Force measurements and filming of physical model swimmers

Prescribed leading edge kinematics of the bar and rod model swimmers were chosen to encompass typical physiological kinematic values and Reynolds numbers for steady swimming hagfish (*Re* 38 000 in hagfish (Lim and Winegard 2015); 22 000 in bar and rod models). After initial explorations of different possible heave and pitch motion programs, we selected one driving actuation program that generated a range of kinematics and that included patterns similar to those observed in freely swimming hagfish. The polyurethane rod and bar were each actuated at a lateral amplitude (defined as half the maximum lateral excursion) of 2 cm and a pitch of ±25°, at frequencies from 0.5 to 2.5 Hz (measured at 0.5 Hz intervals). While in a fixed position in the upstream–downstream direction, each model was actuated over the range of driving frequencies at constant flow speeds of 4.3 cm s^{-1}, 6.5 cm s^{-1}, and 8.9 cm s^{-1} (corresponding to 0.14 BL s^{-1}, 0.21 BL s^{-1}, and 0.29 BL s^{-1}, respectively, where BL = body length = length of the model). Because the two models' respective steady swimming speeds were most clearly indicated (via force measurements described below) at a flow speed of 8.9 cm s^{-1}, and because this higher flow speed corresponds to slow swimming speeds in live hagfish (Lim and Winegard 2015), data collected at this speed were subject to complete analysis and serve as representative data in this paper. Forces and torques exerted by the models were measured in three orthogonal planes using a six-axis force/torque transducer (Nano 17E, ATI Industrial Automation., Apex, NC) attached to the model's leading edge shaft. Force and torque data were phase averaged and imported into LabChart software (v. 7.3.3 ADInstruments, Colorado Springs, CO) where they were combined with data on model position collected from encoders on the mechanical control apparatus. These data were used to calculate mean net axial force exerted by the model, where force measurements above or below zero indicate net thrust or drag, respectively, generated by the model. An occurrence of zero net axial force indicates that the model is swimming steadily at the constant flow tank speed under the condition of self-propulsion (e.g., Lauder *et al* 2011). Power (force *x* velocity) and work per cycle (integral of power with respect to time) exerted by the motor on the model were also calculated, and together with axial force production served as metrics for swimming performance.

To obtain a visual representation of the polyurethane models' undulatory behavior over the range of frequencies prescribed, a high-speed video camera (250 frames s^{-1}, Photron Fastcam PCI1024, 1024 × 1024 pixel resolution, Photron USA Inc., San Diego, CA) aimed at a 45°-angled mirror below the flow tank was used to film ventral views of the swimming models. Two-dimensional (*x*, *y*) coordinates of the model's position over time were recorded from the video images

using a custom Matlab (R2011a, The Mathworks Inc., Natick, MA) program. At intervals of 0.02–0.10 s (dependent on the model's driving frequency) over the course of a complete undulatory cycle, approximately 10 manually digitized points along the length of the model were fitted with a cubic spline to produce a smoothed line representing the model midline at multiple instances in the cycle (see figure 1(c)).

2.4. Hydrodynamics of swimming in physical models and live hagfish

Flow fields around the physical models swimming at 0.5, 1.0, and 2.5 Hz were visualized and quantified with PIV as in our previous work (e.g., Alben 2008, Lauder *et al* 2011, Shelton *et al* 2014, Feilich and Lauder 2015, Lucas *et al* 2015, Quinn *et al* 2015). Neutrally buoyant 50 μm plastic beads (Degussa Corp., Piscataway, NJ) were added to the water in the flow tank, and a continuous argon-ion laser (10 W, Coherent Inc., Santa Clara, CA) aimed through a semi-cylindrical lens produced a thin horizontal light sheet that was positioned at mid-height on the model. A digital high-speed video camera (500 frames s^{-1}, 1024 $\times$ 1024 pixels, Photron USA Inc., San Diego, CA) aimed at a 45°-angled mirror below the clear tank bottom filmed ventral views of the actuated models and the plastic particles in the water as they moved through the light sheet.

Video images were imported into DaVis software (v. 7.2.2, LaVision Inc., Goettingen, Germany), where they were calibrated and processed via an FFT-based cross-correlation routine (two-pass, 16 $\times$ 16 pixel interrogation area with 50% overlap) that analyzed particle movement to produce a two-dimensional array of fluid velocity vectors and vorticity fields. Average free-stream velocity was subtracted from raw vector data to highlight model-generated flows, and obvious erroneous vectors (those that were considerably different from nearest neighbors in magnitude and/or direction) were manually deleted from the vector map. Validated PIV vector maps were analyzed further in a custom Matlab program (written by Eric Tytell, Harvard University 2005) that was used to define and measure flow structures in the model's wake. A fluid jet between two opposite-sign vorticity centers in the wake were assumed to collectively represent a cross-section through a vortex ring, allowing simplified calculations of wake force production (see Drucker and Lauder 1999, Müller *et al* 2001, Tytell and Lauder 2004, Stamhuis and Nauwelaerts 2005). The circulation of this vortex ring was measured as the line integral of the velocity along the jet's main axis through the center of the vortex ring (Tytell and Lauder 2004, Stamhuis and Nauwelaerts 2005). Vortex ring impulse (I_r) was then calculated as:

$$I_r = \tfrac{1}{4}\pi\rho\Gamma h d,$$

where ρ is the fluid density, Γ is the vortex ring circulation, d is the diameter of the vortex ring (approximated as jet diameter), and h is the height of the ring (approximated as the height of the model) (Tytell and Lauder 2004). Previous PIV studies on swimming bodies have demonstrated that vortex ring height closely matches the height of the propulsor (Lauder 2000), such that vortex rings produced by low profile bodies may actually be more oval-shaped than circular (Tytell and Lauder 2004). As the actuated models typically produced a single vortex ring per half cycle, the force generating the ring was estimated as the ring impulse divided by the time period between maximum lateral excursions (Müller *et al* 2001, Tytell and Lauder 2004).

A similar procedure was used to visualize and quantify flows around swimming hagfish for comparison with the bar and rod models. Individual *E. stoutii* were placed in the working section of the seawater-filled flow tank with the laser light sheet positioned approximately 1.5 cm above the floor of the tank as *E. stoutii* tend to swim at the bottom of the tank. Hagfish were prompted to swim by slowly increasing the speed of water flow in the tank or by gently prodding the underside of the hagfish's caudal end. Filmed swimming sequences that were subsequently analyzed consisted of 2–5 consecutive tail beats of steady swimming, defined as less than a 10% change in swim speed over the whole tail beat cycle. The range of steady swimming speeds over which *E. stoutii* voluntarily swam under these conditions was 0.33 to 0.78 BL s^{-1}. PIV vector maps of the hagfish wake were similarly analyzed to identify vortex rings and estimate vortex ring force, which were averaged over multiple tail beats at each swim speed.

For live hagfish, a Spearman's rank correlation test was used to detect a relationship between vortex ring force and swim speed. A Kruskal–Wallis test was performed in JMP Pro 10 (SAS Institute, Inc., Cary, NC) to test for differences in mean vortex ring force produced by live hagfish and the bar and rod models at driving frequencies of 0.5 and 1.0 Hz. Difficulty in detecting discrete wake structures prevented vortex ring measurements at 2.5 Hz.

3. Results

Over the range of driving frequencies tested, few major differences were observed between the elongate polyurethane rod and bar models. The passive behavior of the undulatory wave along the model changed more with the prescribed kinematics than with the shape of the model (figure 3). As actuation frequency increased, wavelength and trailing edge amplitude decreased for both models. Trailing edge amplitudes in the bar model were slightly larger than those observed for the rod model. At the highest tested frequency (2.5 Hz), both models showed an amplitude minimum approximately two-thirds along their length representing a kinematic node. The rod model at 1.0 Hz showed the greatest kinematic similarities to swimming hagfish

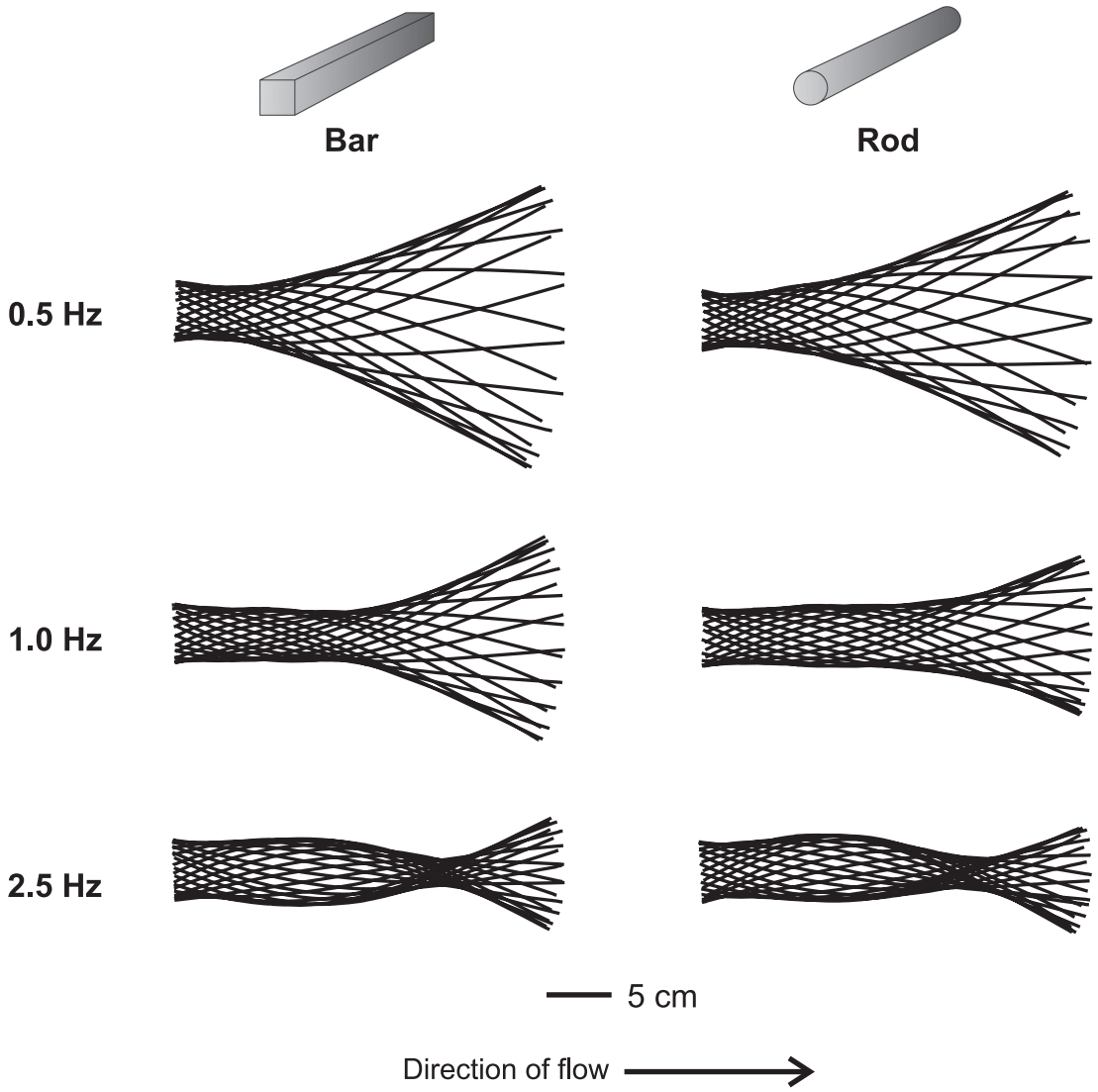

Figure 3. Ventral midline drawings of the polyurethane bar and rod models being actuated at select driving frequencies. Heave (lateral) amplitude = 2 cm, pitch angle = 25°. A series of traced midlines from sequential instances in time (each separated by $\Delta t = 0.1$ s at 0.5 Hz; 0.05 s at 1.0 Hz; 0.02s at 2.5 Hz) are overlaid on top of one another to indicate the lateral amplitude envelope for a typical whole undulatory cycle. For each model, the leading edge is at the left and water flow is from left to right at 8.9 cm s^{-1}. For both the rod and bar, trailing edge amplitude and wavelength tended to decrease with increasing driving frequency, with a nodal point appearing at frequencies above 2 Hz. The 5 cm scale bar applies to all midline drawings.

body movement (compare figure 3, 1.0 Hz for the rod model, to figure 1(c) hagfish kinematics).

Net thrust production, measured by the force transducer attached to the model shaft, generally increased with increasing driving frequency and varied between models at certain frequencies (figure 4(a)). At frequencies below 1.5 Hz, the square bar generated more thrust than the round rod. Accordingly, the point of zero net thrust, and therefore the steady swimming self-propelled speed equal to the fixed flow speed (8.9 cm s^{-1}), occurred at a lower driving frequency for the bar than the rod. At frequencies greater than 1.5 Hz, however, the rod produced slightly more thrust compared to the bar, and 1.5 Hz represented a cross-over point where the relative performance of the bar and rod changed (figure 4(a)). Meanwhile, the work required per cycle to actuate each model was always greater for the square bar than the round rod, and tended to increase only at higher driving frequencies (figure 4(b)).

PIV vector maps demonstrate that wake structure in the plane of oscillation was also similar between the bar and rod models (figures 5 and 6). When actuated at 1.0 Hz, the wake produced by each model resembles a 2*P* wake structure, where two pairs of vortices are shed per cycle (Hultmark *et al* 2007, Schnipper *et al* 2009). Between each pair of counter-rotating vortices a laterally directed fluid jet with little downstream momentum is evident (open white arrows, figures 5 and 6). The vorticity shed into the wake by the square bar tends to be lower and less visually apparent than the vorticity generated at the bar's sharp trailing edges,

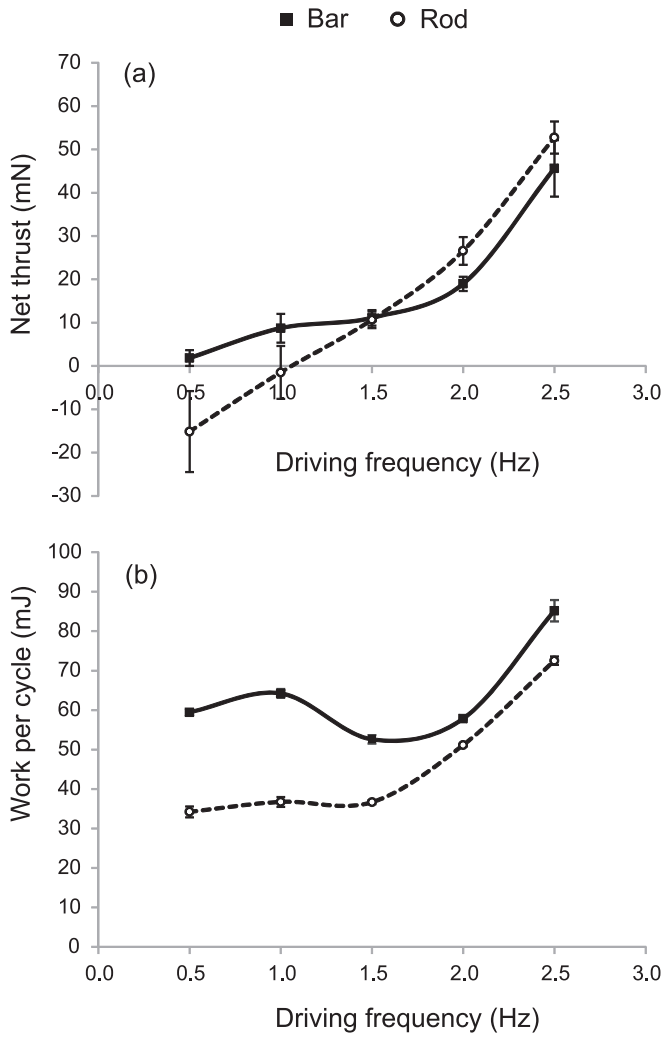

Figure 4. (a) Net thrust and (b) work per cycle as a function of driving frequency for the polyurethane bar (solid square symbols) and rod (open circle symbols); models were actuated in a flow tank with a constant flow speed of 8.9 cm s^{-1}. Values are averaged over a complete undulatory cycle; error bars are one standard error of the mean (some bars are small and do not extend beyond symbol edges). Net thrust (a) generally increases with increasing frequency, but differences between the rod and bar models depend on the driving frequency. Work per cycle (b) is always higher for the bar than the rod regardless of driving frequency, suggesting that cylindrical bodies may be able to exploit reduced energy requirements while still producing thrust.

however (figure 6). As patterns of bending within each model changed more with differences in driving frequency than differences in shape, patterns of flow around the models similarly varied the most over changes in kinematics. At a driving frequency of 0.5 Hz, high amplitude motions of the models' posterior regions drew a broad mass of fluid toward each model, and lateral flows induced by the flat-sided bar were slightly stronger than for the rod (figures 7(a) and (b)). At 2.5 Hz, however, the wake no longer retained a 2*P* structure with distinct lateral jets but became less organized for both models (figures 7(c) and (d)).

In contrast, the wake of steady swimming Pacific hagfish had a 2*P* arrangement for all swimming speeds observed in this study (figure 8 shows a representative wake). Central fluid jets associated with vortex rings shed into the hagfish wake were caudo-laterally directed, and vortex ring force calculated from the wake vorticity was independent of swim speed (Spearman's $r_s = 0.20$, $P = 0.70$) over the relatively narrow range of swimming speeds analyzed here. For the bar and rod models, the force associated with presumptive vortex rings shed into the wake at 0.5 and 1.0 Hz appeared to differ between frequencies, with both bar and rod models producing forces two to three times higher than forces calculated for swimming hagfish (figure 9); however, a Kruskal–Wallis test did not detect statistically significant differences in mean vortex ring force among the models and hagfish ($K = 9.35$, $P = 0.053$).

4. Discussion

This study examined undulatory swimming behavior in two flexible physical models that approximate the three-dimensional morphology of hagfish anguilliform swimmers while still retaining a simple, uniform shape. The physical models were externally actuated only at

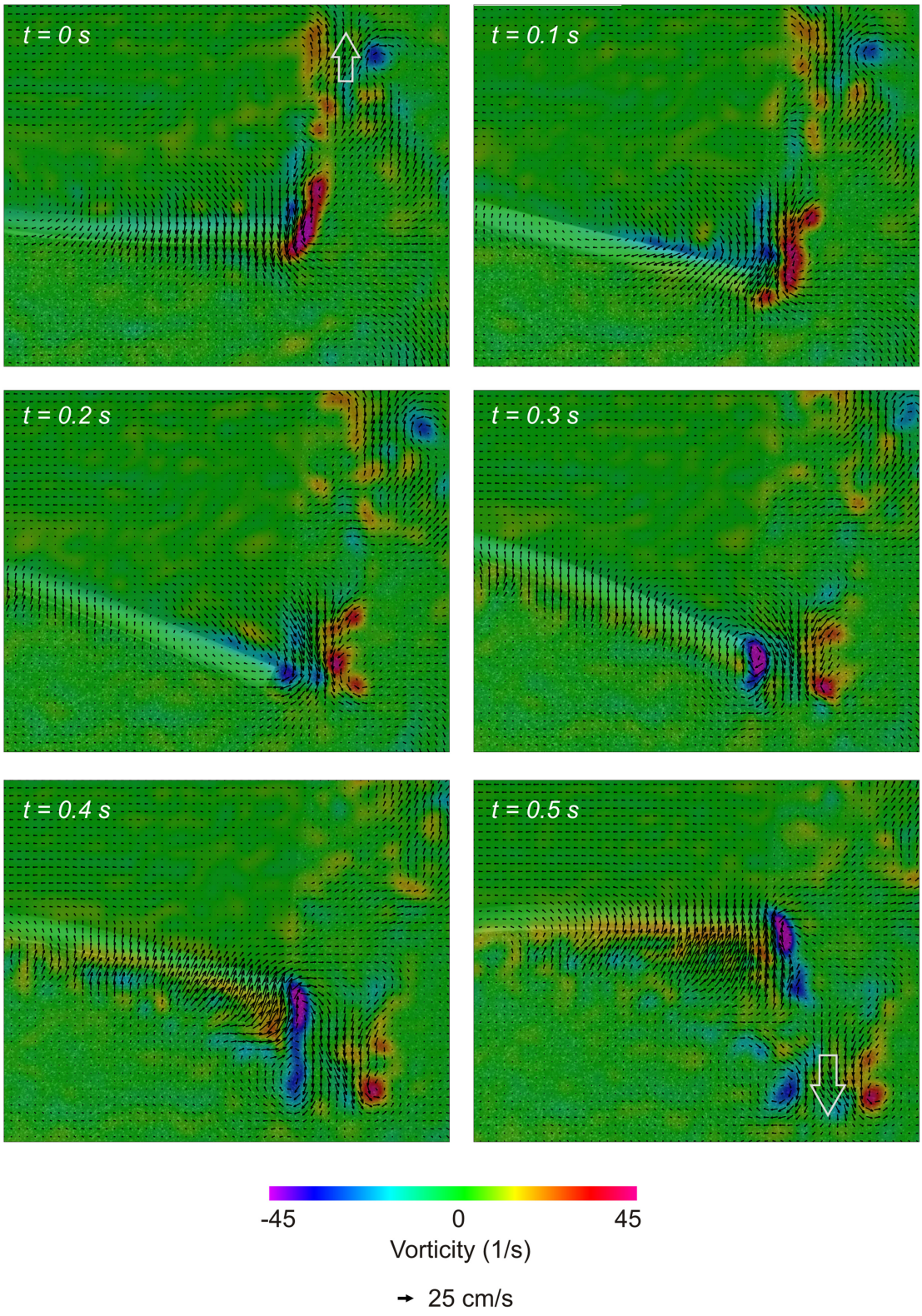

Figure 5. Representative time-series of horizontal-view flows generated by the polyurethane rod model being actuated at a driving frequency of 1.0 Hz in a flow tank with a constant flow speed of 8.9 cm s^{-1}. Heave (lateral) amplitude = 2 cm; pitch angle = 25°. Fluid velocity vectors are represented by black arrows, and the vorticity field is color-coded. Only every second vector is shown for clarity. Water flow is from left to right and the freestream velocity has been subtracted from the flow. At this frequency, the actuated rod has a 2*P* wake. A pair of vortices with a central fluid jet (large open arrows) is visible at $t = 0$ s and $t = 0.5$ s. The fluid jets are laterally directed, with little visible downstream momentum. This overall wake morphology is similar to that observed for the polyurethane bar model at the same driving frequency (figure 6).

their leading edge, which generated undulatory waves along the model that passively propagated toward the trailing edge. The motion of the model is a result of interactions between the input kinematics, the model's inherent mechanical properties, and external forces from the surrounding fluid (Alben 2008). In live

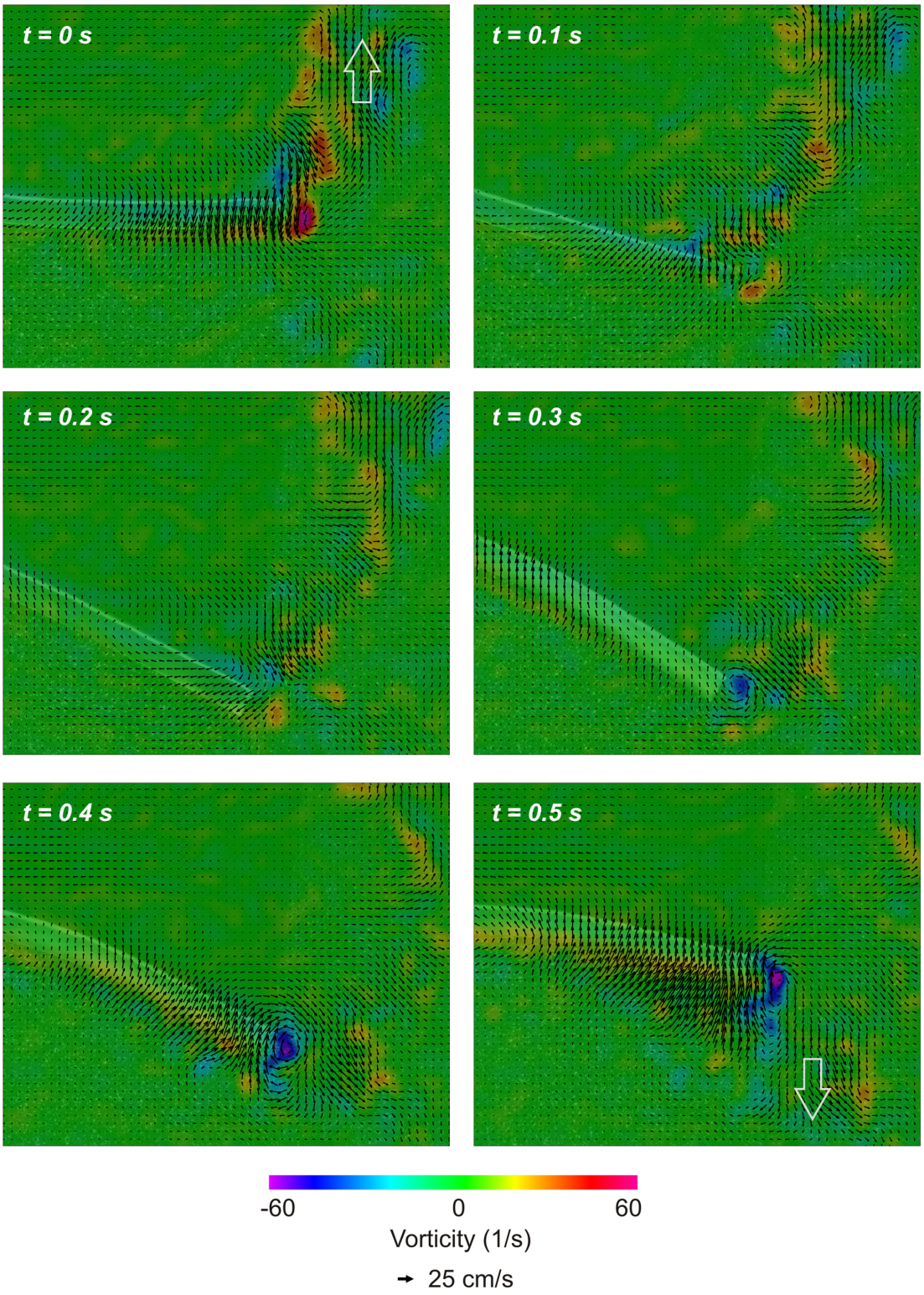

Figure 6. Representative time-series of horizontal-view flows generated by the polyurethane bar model being actuated at a driving frequency of 1.0 Hz in a flow tank with a constant flow speed of 8.9 cm s^{-1}. Heave (lateral) amplitude = 2 cm; pitch angle = 25°. Fluid velocity vectors are represented by black arrows, and the vorticity field is color-coded. Only every second vector is shown for clarity. Water flow is from left to right and the freestream velocity has been subtracted from the flow. At this frequency, the actuated bar has a 2*P* wake. Centers of opposite-sign vorticity on either side of a fluid jet (large open arrows) are visible at $t = 0$ s and $t = 0.5$ s. The fluid jets are laterally directed, with minimal downstream momentum. This overall wake morphology is similar to that observed for the polyurethane rod model at the same driving frequency (figure 5).

anguilliform swimmers, an additional determinant of body motion arises from the pattern of active muscular contraction along the length of the body (Gillis 2000, Tytell *et al* 2010). Here, we compare the swimming behavior of the physical models to known characteristics of swimming in hagfish and other elongate anguilliform swimmers to better understand mechanisms of undulatory locomotion.

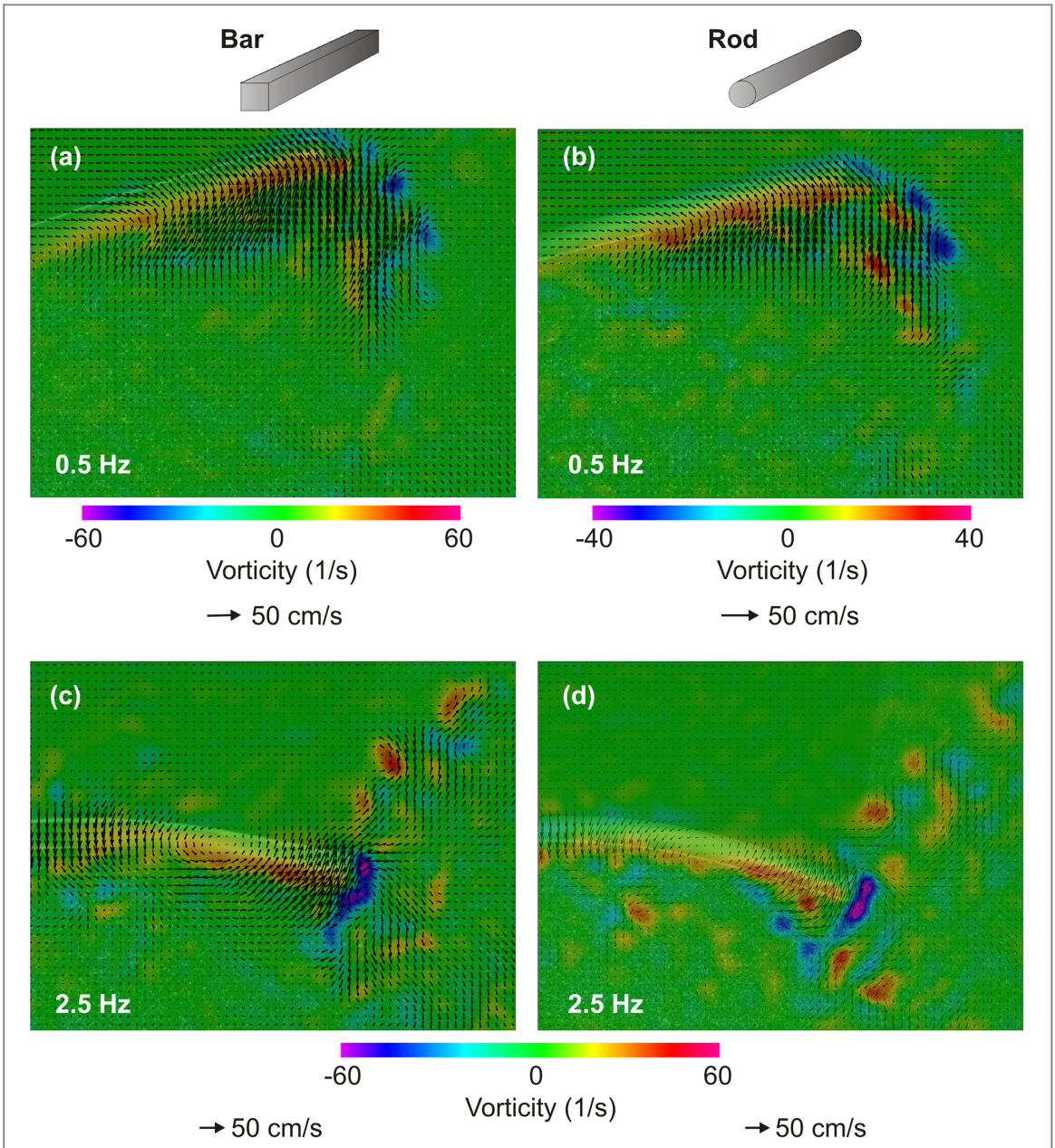

Figure 7. Ventral views of representative flow fields around the polyurethane (a), (c) bar and (b), (d) rod models being actuated at (a), (b) 0.5 Hz and (c), (d) 2.5 Hz in a flow tank with a constant flow speed of 8.9 cm s^{-1}. Fluid velocity vectors are represented by black arrows, and the vorticity field is color-coded. Only every second vector is shown for clarity. Water flow is from left to right and the freestream velocity has been subtracted from the flow. Note the different scales for velocity vectors and vorticity beneath each image. Wake structure is influenced more by driving frequency than by differences in model shape. At 0.5 Hz (a) and (b), the models generate distinct lateral flows, while at 2.5 Hz (c) and (d), the wake has lost its coherent 2*P* structure for both models.

The shape of the undulatory wave along the polyurethane models was strongly influenced by driving frequency (figure 3), and changes in waveform shape are explained well by mechanical theory. For a body of uniform stiffness, the speed of an undulatory wave along the body remains constant (McHenry *et al* 1995). Because wave speed is equal to the product of wavelength and frequency, an increase in frequency is accompanied by a decrease in wavelength. This was observed in both the bar and rod model, where increases in driving frequency resulted in decreases in wavelength as well as trailing edge amplitude (figure 3). McHenry and his colleagues (McHenry *et al* 1995) similarly studied undulatory waves in physical models of pumpkinseed sunfish (*Lepomis gibbosus*) and found that tail beat amplitude also decreased with increasing driving frequency. Despite lacking additional active musculature along their length to power swimming motions, the flexible physical models studied here reproduced certain aspects of undulatory swimming also found in live swimming hagfish. The pattern of lateral excursion along the body was similar between Pacific hagfish (figure 1(c)) and the bar and rod models (figure 3) undulating at similar frequencies (~1 Hz). In addition, Pacific hagfish also reduce their tail beat amplitude and wavelength while increasing tail beat

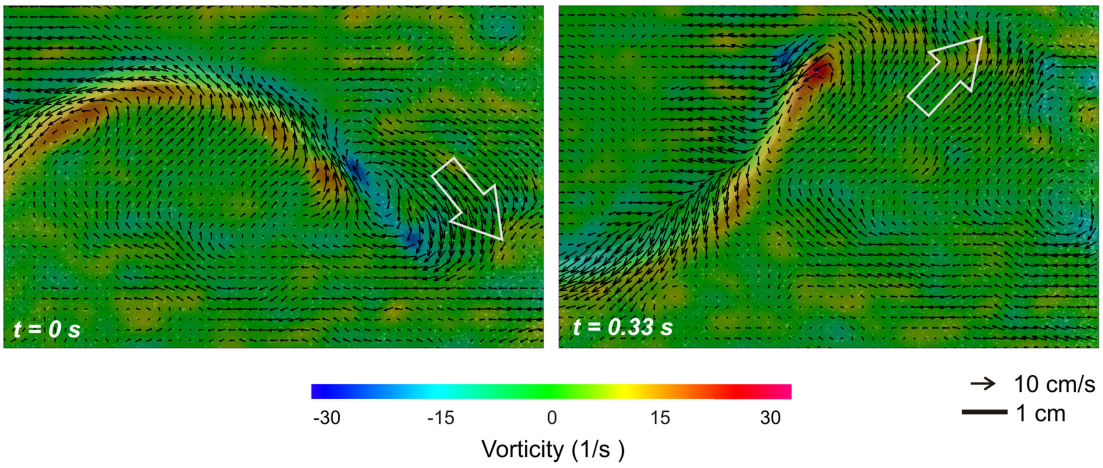

Figure 8. Ventral views of representative flow fields around a free-swimming Pacific hagfish (BL = 23.0 cm, swim speed 0.33 BL s^{-1}). Fluid velocity vectors are represented by black arrows, and the vorticity field is color-coded. Only every second vector is shown for clarity. Water flow is from left to right and the freestream velocity has been subtracted from the flow. In contrast to the bar and rod models, the hagfish steady swimming wake had a coherent 2*P* structure with caudo-laterally directed fluid jets (open white arrows) for all swim speeds observed in this study.

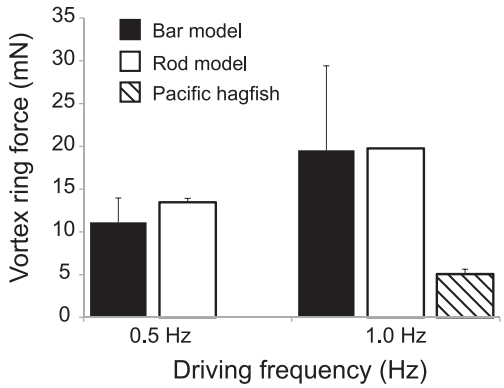

Figure 9. Mean force calculated for vortex rings (counter-rotating vortices with a central jet) shed into the wake of the polyurethane bar (solid bars) and rod (open bars) models being actuated at 0.5 and 1.0 Hz in a flow tank with a constant flow speed of 8.9 cm s^{-1}. Representative mean vortex ring force data for a Pacific hagfish (diagonal striped bar) swimming with a tail beat frequency of 0.9 Hz are also shown for comparison. Error bars are one standard error of the mean (the error bar for the rod model at 1.0 Hz is small and does not extend beyond the bar graph edge). The polyurethane models tended to generate larger wake vortex ring forces than the freely swimming hagfish, but these differences were not statistically significant.

frequency to swim at faster steady swim speeds (Lim and Winegard 2015), suggesting that these particular kinematic changes in their undulatory wave could be entirely passive. Long *et al* (2002) also noticed a decrease in tail beat amplitude in hagfish with increasing frequency.

However, other features of the polyurethane models' waveform and wake morphology suggest where live swimmers might be actively modulating their body motion or mechanical properties. In the bar and rod models, a minimum in undulatory amplitude passively develops in the posterior body region as driving frequency reaches 2.5 Hz (figure 3). In contrast, for many live elongate anguilliform swimmers, an amplitude minimum commonly occurs near the head, where it remains even over a broad range of swimming speeds or tail beat frequencies (Gillis 1997, Gillis 1998, Lim and Winegard 2015). This bending pattern observed in the models may potentially be related to the loss of a coherent 2*P* wake structure as driving frequency increased from 1.0 to 2.5 Hz, and possibly indicate that the models are oscillating at a higher mode (figures 5, 6, 7(c) and (d)). Wake structure can be influenced by the shape of a body's undulatory wave, particularly at posterior regions (Anderson *et al* 1998, Tytell *et al* 2010, Leftwich *et al* 2012). For all swim speeds and kinematic combinations observed in voluntarily swimming hagfish, a coherent 2*P* wake was always observed (see figure 8 for a representative wake), suggesting some active control of the shape of the body undulatory wave (Long and Nipper 1996, Long *et al* 2010). It should be noted, however, that the maximum tail beat frequency reached by hagfish in the present study was lower than 2.5 Hz.

Estimated vortex ring force did not differ between the rod and bar at low frequencies, though the models tended to produce greater vortex ring forces than freely swimming hagfish (figure 9). This difference in force magnitude is likely due to the physical models having higher flexural stiffness than live hagfish, but the functional significance of the difference is as yet unclear. Components of these vortex ring forces that are caudally directed would contribute to forward thrust, but components that are laterally directed would not (Tytell and Lauder 2004). In the present study, the hagfish wake consisted of fluid jets that are caudo-laterally directed (figure 8), while the rod and bar wakes exhibited relatively strong laterally directed flows (figures 5–7). Even with information on fluid jet angle, however, wake flow patterns alone are not

necessarily reliable indicators of thrust for elongate undulating bodies. For instance, the wakes of steadily swimming eels have been shown to consist of laterally directed fluid jets with little downstream momentum visible as rearward flows (Müller *et al* 2001, Tytell and Lauder 2004). In this study, strong laterally directed flows were still observed in flapping rod and bar wakes when the models were producing considerable net thrust as evidenced by the force data (figures 7(c), (d) and 4(a)). When three-dimensional bodies are generating flows, as in live fish and the rod and bar models, out-of-plane motion that is not captured in two-dimensional flow fields may be responsible for some thrust production, as well. Dabiri (2005, 2006) also discussed several reasons why wake vortex formation may not accurately represent thrust production and suggested alternative methods of analysis.

Model shape (bar versus rod) appeared to have a minimal effect on general patterns of body waveform and wake morphology, but differences between the rod and bar models arose in measurements of their respective thrust production and work (figure 4). The different cross-sectional shapes of these models is relevant to anguilliform swimming because the lateral surfaces of an elongate swimming body push on the water and propel the body through it via fluid reaction forces. A surface with a rounded profile (i.e., rod model) should have smaller drag and added mass coefficients than a profile with a flat surface (i.e., bar model) (Vogel 1994), potentially producing smaller fluid forces and thrust. Interestingly, differences in thrust production between the bar and rod models were dependent on the driving frequency. At low frequencies, the flat-sided bar generated more net thrust, while at higher frequencies, the rod and bar models generated approximately equal amounts of net thrust (figure 4(a)).

In contrast, the work exerted to actuate the models was always greater in the bar than the rod (figure 4(b)). Differences between the models in energetic cost and net thrust production could be due to the higher bending rigidity and inertia of the bar, in addition to cross-sectional shape and consequent differing three-dimensional flow patterns around the body. Our results cannot discriminate among these causes, but nonetheless have implications for live anguilliform swimmers. Because the rod and bar still produced comparable amounts of net thrust, this suggests that flexible, cylindrically shaped swimmers (e.g., eels, hagfish, salamanders, and sea snakes) can exploit reduced energy requirements to move their bodies through the water while still generating thrust along the entire length of their bodies and achieving reasonable swim speeds. Lateral compression of tails in live anguilliform swimmers further confers savings in energy, as tapering tails require less force and energy to move (McMillen and Holmes 2006), but body regions that are necessarily cylindrical (due to anatomical and/or phylogenetic constraints) may also generate thrust and contribute to forward propulsion. Furthermore, the work required to actuate the bar and rod models changed little over increasing driving frequencies spanning 0.5–1.5 Hz (figure 4(b)), demonstrating that it is possible to exploit passive changes in emergent body motion and produce more propulsive force without incurring greater energetic costs.

In accordance with other studies that used physical models to study swimming in flexible bodies (McHenry *et al* 1995, Root *et al* 1999), we support the hypothesis that anterior muscle activation on its own could conceivably power undulatory locomotion in highly flexible bodies with minimal internal stiffening elements, such as that of the hagfish (Blight 1977). Our experimental analysis of undulatory swimming behavior in 3D anguilliform models expands on findings from previous studies of anguilliform swimming robots. Root and his colleagues (Root *et al* 1999) quantified propulsive wave characteristics in simple physical models with varying stiffnesses for comparison with live, free-swimming lamprey (*Petromyzon marinus*), but the models were actuated at a single frequency of 12 Hz, much higher than undulation frequencies commonly observed in elongate anguilliform swimmers (e.g., hagfish (Long *et al* 2002), eels (Gillis 1998, Tytell 2004), and swimming snakes (Jayne 1985, Munk 2008)). Leftwich *et al* (2012) used a lamprey-like 3D robotic swimmer to study how thrust production and wake morphology change with tail stiffness during anguilliform swimming. This model swam at relatively low frequencies (0.1–0.65 Hz), and was actuated over a large portion of its length, so that passive flexion was restricted to the tail. The present study has shown that increasing contraction frequency of muscles only near the head could affect body motion at the tail, and consequently swim performance, if the body can transmit the forces along its length.

5. Conclusions

In the present study, 3D flexible physical models approximating elongate anguilliform swimmers, specifically the hagfish, were actuated at their leading edge and capable of generating thrust from passively propagated 'body' waves. Patterns of body bending and wake morphology were similar between free-swimming Pacific hagfish and the uniformly shaped models (a round rod and square rod) undulating at frequencies of approximately 1 Hz. However, differences between the flexible models and live hagfish in axial bending patterns and wake morphology might inform hypotheses on how active muscular control specifically influences anguilliform and other modes of undulatory locomotion. We found that physical models with identical projected area but minor variations in cross-sectional shape, flexural stiffness, and mass, can generate comparable amounts of thrust

while incurring different amounts of work. Additional factors influencing undulatory swim performance may be systematically explored by adapting the 3D models used here, and future experiments should use models with morphologies and mechanical properties that increasingly approach that of live elongate anguilliform swimmers. These simple models are easily modified to test the effects of body cross-section, tapering, and changes in structural properties, for example, on the passive behavior of body undulatory waves.

Acknowledgments

Many thanks to Chuck Witt and Eric Tytell for providing invaluable Matlab code. We also thank Vern Baker, Chuck Witt, and Dan Quinn for assistance during data collection, and Erin Blevins and Li Wen for constructive discussions about this experiment and analysis. This project was supported by National Science Foundation (NSF) grant EFRI-0938043 and by Office of Naval Research (ONR) MURI Grant N000141410533 monitored by Dr Bob Brizzolara to George Lauder, the Harvard University Organismic and Evolutionary Biology Department, and a Robert A. Chapman Memorial Scholarship granted to Jeanette Lim.

References

Alben S 2008 Optimal flexibility of a flapping appendage in an inviscid fluid *J. Fluid Mech.* **614** 355–80

Anderson J M, Streitlein K, Barrett D and Triantafyllou M S 1998 Oscillating foils of high propulsive efficiency *J. Fluid Mech.* **360** 41–72

Blevins E L and Lauder G V 2013 Swimming near the substrate: a simple robotic model of stingray locomotion *Bioinsp. Biomim.* **8** 016005

Blight A R 1977 The muscular control of vertebrate swimming movements *Biol. Rev.* **52** 181–218

Brischoux F and Shine R 2011 Morphological adaptations to marine life in snakes *J. Morph.* **272** 566–72

Carlson R L and Lauder G V 2011 Escaping the flow: boundary layer use by the darter *Etheostoma Tetrazonum* (Percidae) during benthic station holding *J. Exp. Biol.* **214** 1181–93

Curet O M, Patankar N A, Lauder G V and MacIver M A 2011 Mechanical properties of a bio-inspired robotic knifefish with an undulatory propulsor *Bioinsp. Biomim.* **6** 026004

Dabiri J O 2005 On the estimation of swimming and flying forces from wake measurements *J. Exp. Biol.* **208** 3519–32

Dabiri J O 2006 Note on the induced Lagrangian drift and added-mass of a vortex *J. Fluid Mech.* **547** 105–13

Dabiri J O, Bose S, Gemmell B J, Colin S P and Costello J H 2014 An algorithm to estimate unsteady and quasi-steady pressure fields from velocity field measurements *J. Exp. Biol.* **217** 331–6

Dewey P A, Boschitsch B M, Moored K W, Stone H A and Smits A J 2013 Scaling laws for the thrust production of flexible pitching panels *J. Fluid Mech.* **732** 29–46

Drucker E G and Lauder G V 1999 Locomotor forces on a swimming fish: three-dimensional vortex wake dynamics quantified using digital particle image velocimetry *J. Exp. Biol.* **202** 2393–412

Emerson S, Travis J and Koehl M A R 1990 Functional complexes and additivity in performance: a test case with flying frogs *Evolution* **44** 2153–7

Feilich K L and Lauder G V 2015 Passive mechanical models of fish caudal fins: effects of shape and stiffness on self-propulsion *Bioinsp. Biomim.* **10** 036002

Gemmell B J, Colin S P, Costello J H and Dabiri J O 2015 Suction-based propulsion as a basis for efficient animal swimming *Nat. Commun.* **6** 8790

Gillis G B 1997 Anguilliform locomotion in an elongate salamander (Siren intermedia): effects of speed on axial undulatory movements *J. Exp. Biol.* **200** 767–84

Gillis G B 1998 Environmental effects on undulatory locomotion in the American eel *Anguilla rostrata*: kinematics in water and on land *J. Exp. Biol.* **201** 949–61

Gillis G B 2000 Patterns of white muscle activity during terrestrial locomotion in the American eel (*Anguilla rostrata*) *J. Exp. Biol.* **203** 471–80

Hart J L 1973 Pacific fishes of Canada *Fish. Res. Board Can. Bull.* **180** 1–740

Hultmark M, Leftwich M and Smits A J 2007 Flowfield measurements in the wake of a robotic lamprey *Exp. Fluids* **43** 683–90

Jayne B C 1985 Swimming in constricting (*Elaphe g. guttata*) and nonconstricting (*Nerodia fasciata pictiventris*) colubrid snakes *Copeia* **1985** 195–208

Johansson L C and Norberg R A 2003 Delta-wing function of webbed feet gives hydrodynamic lift for swimming propulsion in birds *Nature* **424** 65–8

Koehl M A 2003 Physical modelling in biomechanics *Phil. Trans. R. Soc.* B **358** 1589–96

Koehl M A R, Evangelista D and Yang K 2011 Using physical models to study the gliding performance of extinct animals *Int. Comp. Biol.* **51** 1002–18

Lauder G V 2000 Function of the caudal fin during locomotion in fishes: kinematics, flow visualization, and evolutionary patterns *Am. Zool.* **40** 101–22

Lauder G V, Lim J L, Shelton R, Witt C, Anderson E J and Tangorra J L 2011 Robotic models for studying undulatory locomotion in fishes *Mar. Technol. Soc. J.* **45** 45–55

Leftwich M C, Tytell E D, Cohen A H and Smits A 2012 Wake structures behind a swimming robotic lamprey with a passively flexible tail *J. Exp. Biol.* **215** 416–25

Lim J and Winegard T 2015 Diverse anguilliform swimming kinematics in Pacific hagfish (*Eptatretus stoutii*) and Atlantic hagfish (*Myxine glutinosa*) *Can. J. Zool.* **93** 213–23

Lindsey C C 1978 Form, function, and locomotory habits in fish *Fish Physiology: Locomotion* ed W S Hoar and D J Randall vol 7 (New York: Academic) pp 1–100

Long J H 1998 Muscles, elastic energy, and the dynamics of body stiffness in swimming eels *Am. Zool.* **38** 771–92

Long J H, Hale M E, McHenry M J and Westneat M W 1996 Functions of fish skin: flexural stiffness and steady swimming of longnose gar Lepisosteus osseus *J. Exp. Biol.* **199** 2139–51

Long J H, Koob-Emunds M, Sinwell B and Koob T J 2002 The notochord of hagfish *Myxine glutinosa*: visco-elastic properties and mechanical functions during steady swimming *J. Exp. Biol.* **205** 3819–31

Long J H and Nipper K S 1996 The importance of body stiffness in undulatory propulsion *Am. Zool.* **36** 678–94

Long J H, Porter M E, Root R G and Liew C W 2010 Go reconfigure: how fish change shape as they swim and evolve *Integr. Comp. Biol.* **50** 1120–39

Lucas K N, Thornycroft P, Gemmell B J, Colin S P, Costello J H and Lauder G V 2015 Effects of non-uniform stiffness on the swimming performance of a passively-flexing, fish-like foil model *Bioinsp. Biomim.* **10** 056019

McHenry M J, Pell C A and Long J H 1995 Mechanical control of swimming speed: stiffness and axial wave form in undulating fish models *J. Exp. Biol.* **198** 2293–305

McMillen T and Holmes P 2006 An elastic rod model for anguilliform swimming *J. Math. Biol.* **53** 843–86

Moored K W, Dewey P A, Smits A J and Haj-Hariri H 2012 Hydrodynamic wake resonance as an underlying principle of efficient unsteady propulsion *J. Fluid Mech.* **708** 329–48

Müller U K, Smit J, Stamhuis E J and Videler J J 2001 How the body contributes to the wake in undulatory fish swimming: flow fields of a swimming eel (*Anguilla anguilla*) *J. Exp. Biol.* **204** 2715–62

Munk Y 2008 Kinematics of swimming garter snakes (*Thamnophis sirtalis*) *Comp. Biochem. Physiol.* A **150** 131–5

Ota K G, Fujimoto S, Oisi Y and Kuratani S 2011 Identification of vertebra-like elements and their possible differentiation from sclerotomes in the hagfish *Nat. Commun.* **2** 373

Quinn D B, Lauder G V and Smits A J 2014 Flexible propulsors in ground effect *Bioinsp. Biomim.* **9** 1–9

Quinn D B, Lauder G V and Smits A J 2015 Maximizing the effciency of a flexible propulsor using experimental optimization *J. Fluid Mech.* **767** 430–48

Richards C T and Clemente C J 2012 A bio-robotic platform for integrating internal and external mechanics during muscle-powered swimming *Bioinsp. Biomim.* **7** 016010

Root R G, Courtland H W, Pell C A, Hobson B, Twohig E J, Suter R B, Shepherd W R I, Boetticher N C and Long J H 1999 Swimming fish and fish-like models: the harmonic structure of undulatory waves suggest that fish actively tune their bodies *Proc. 11th Int. Symp. on Unmanned Untethered Submersible Technology* vol 11 (Autonomous Undersea Systems Institute) pp 378–88

Schlichting H 1979 *Boundary-Layer Theory* (New York: McGraw-Hill)

Schnipper T, Andersen A and Bohr T 2009 Vortex wakes of a flapping foil *J. Fluid Mech.* **633** 411–23

Scott W B and Scott M G 1988 Atlantic fishes of Canada *Can. Bull. Fish. Aquat. Sci.* **219** 1–731

Shelton R M, Thornycroft P J M and Lauder G V 2014 Undulatory locomotion of flexible foils as biomimetic models for understanding fish propulsion *J. Exp. Biol.* **217** 2110–20

Stamhuis E J and Nauwelaerts S 2005 Propulsive force calculations in swimming frogs: II. Application of a vortex ring model to DPIV data *J. Exp. Biol.* **208** 1445–51

Tangorra J L, Lauder G V, Hunter I W, Mittal R, Madden P G A and Bozkurttas M 2010 The effect of fin ray flexural rigidity on the propulsive forces generated by a biorobotic fish pectoral fin *J. Exp. Biol.* **213** 4043–54

Tytell E D 2004 The hydrodynamics of eel swimming: II. Effect of swimming speed *J. Exp. Biol.* **207** 3265–79

Tytell E D, Hsu C-Y, Williams T L, Cohen A H and Fauci L J 2010 Interactions between internal forces, body stiffness, and fluid environment in a neuromechanical model of lamprey swimming *Proc. Natl Acad. Sci. USA* **107** 19832–19837s

Tytell E D and Lauder G V 2004 The hydrodynamics of eel swimming: I. Wake structure *J. Exp. Biol.* **207** 1825–41

Vogel S 1994 *Life in Moving Fluids: The Physical Biology of Flow* (Princeton: Princeton University Press)

Webb P W 1975 Hydrodynamics and energetics of fish propulsion *Bull. Fish. Res. Board Can.* **190** 1–159

Wen L, Wang T M, Wu G H and Liang J H 2012 Hydrodynamic investigation of a self-propelled robotic fish based on a force-feedback control method *Bioinsp. Biomim.* **7** 036012

Williams T L and McMillen T 2015 Strategies for swimming: explorations of the behaviour of a neuro-musculo-mechanical model of the lamprey *Biol. Open* **4** 253–8

Witt W C, Wen L and Lauder G V 2015 Hydrodynamics of *c*-start escape responses of fish as studied with simple physical models *Integr. Comp. Biol.* **55** 728–39